J Mol Model (2005) 11: 407–415
DOI 10.1007/s00894-005-0270-9

ORIGINAL PAPER

Jerzy Ciarkowski · Magdalena Witt · Rafał Ślusarz

A hypothesis for GPCR activation

Received: 28 October 2004 / Accepted: 17 February 2005 / Published online: 12 May 2005

Abstract Growing evidence that rhodopsin (RD) and related G protein-coupled receptors form functional dimers/oligomers, followed by direct proof (using atomic force microscopy) that in the retina disc membrane RD associates into a paracrystalline network of rows of dimers, need models of the RD-transducin (Gt) complex that would envision an optimal RD dimer/oligomer able to satisfy all well-documented interactions with Gt. Of the models proposed so far, only a few refer to RD dimers and only one of them proposes a complex of Gt with an RD oligomer (Filipek S, Krzyśko KA, Fotiadis D, Liang Y, Saperstein DA, Engel, A, Palczewski K Photochem Photobiol Sci 3: 628–638, 2004). This paper puts forward a hypothesis on another arrangement of RD monomers into the reported network of rows of dimers. Arguments for the compatibility of this set-up with interactions and activation of RD in the complex with Gt, in particular, with the well-documented movement of transmembrane helix 6 and cytosolic loop 3, which is vital for RD activation, are provided and discussed.

Keywords Class A · GPCR activation · G protein · Gt · rhodopsin · transducin

Abbreviations 7TM: Transmembrane heptahelical bundle · AFM: Atomic force microscopy · CL'N': Cytosolic loop 'N' · EL'N': Extracellular loop 'N' · G(αβγ): G protein, the guanine nucleotide-binding protein · Gα(βγ): G protein α(βγ, respectively) subunit · GPCR: G protein-coupled receptor · Gt(αβγ): Gt protein, transducin · OT(R): Oxytocin (receptor) · RD: "Dark" inactive rhodopsin · RD*: Meta II (MII) activated rhodopsin · TM'N': Transmembrane helices 'N' · VP: Vasopressin

J. Ciarkowski (✉) · M. Witt · R. Ślusarz
University of Gdańsk, Faculty of Chemistry, ul,
Sobieskiego 18, 80-952 Gdańsk, Poland
E-mail: jurek@chem.univ.gda.pl
Tel.: +4858-345-0330
Fax: +4858-341-0357

Introduction

Recently, evidence has been growing that G protein-coupled receptors (GPCRs) Class A commonly form functional (di/oligo)mers [1–6]. It has also been proven, using atomic force microscopy (AFM), that their best-studied representative rhodopsin (RD) tends to organize itself in the disk membrane into a paracrystalline array of rows of dimers [7–9]. A molecular model of the arrangement of the high-resolution RD monomers (Protein Data Bank (PDB) [10] entry 1HZX [11]) into this array was proposed. It was termed the "IV–V model", reflecting its most prominent feature i.e., that transmembrane helices 4 and 5 (TM4–5) from two neighboring 1HZX monomers make a tight interface within the dimers of local C2-symmetry [8, 9], PDB entry 1N3M, Fig. 1a. The model perfectly met the intra-dimer and between-dimer distances, both equal to 38 Å, as well as the distance between the double rows, found from AFM to be 84 Å, implying a 46 Å distance between the nearest neighbors from different rows. A mode of association of transducin (Gt) to RD, as implemented in this arrangement, was also proposed [12], Fig. 1a. Playing with the arrangements typical of 1N3M leads to the notion that an RD monomer will fit into the AFM lattice, provided the longer axis of its ellipse-like projection onto the extradiscal surface slopes ~45° relative to the dimers' progression axis, Fig. 1. It is this ellipse-like shape of the RD projection and the tightness of packing of the dimers into the rows (within the 38 Å×38 Å framework) that imposes the ~45° slope. If one attributes to the explicit ellipse in Fig. 1a the "−45° slope" then its C_2-symmetrically related counterpart will make a "135° slope", while in Fig. 1b the monomer arrangement would accordingly consist of the "45°/225°

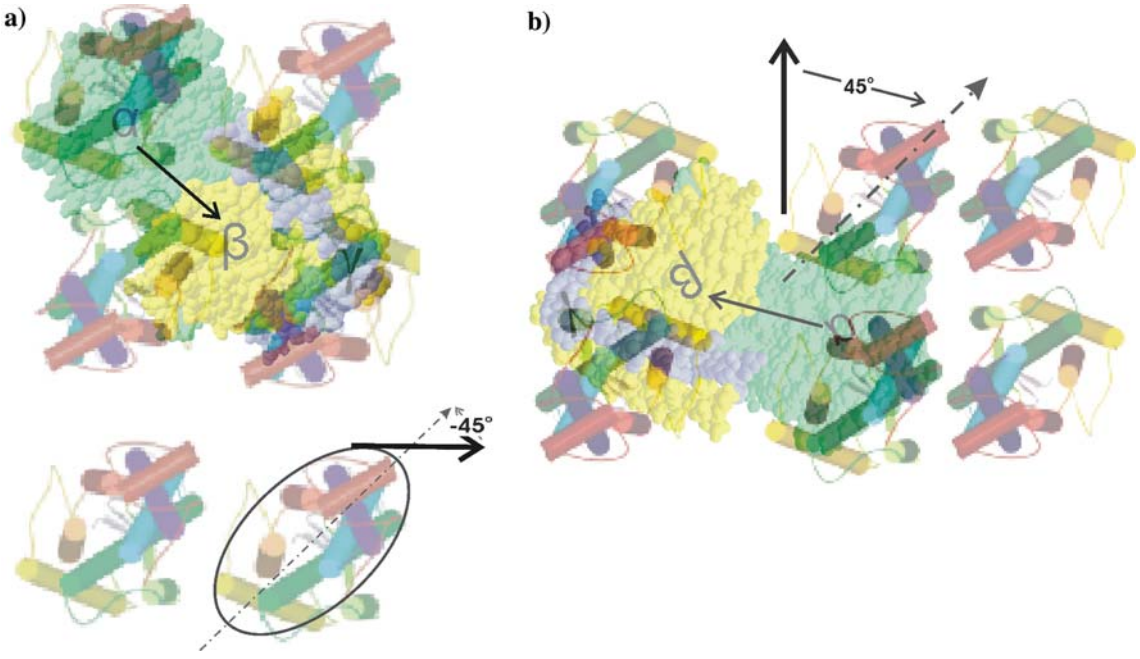

Fig. 1 Overview of the RD monomer arrangements in the experimentally observed rows of dimmers [8] in the complex with Gt.**a** The hypothesis published [12]. **b** The current hypothesis. It differs from **a** by the clockwise ~90° rotation of RD monomers in the 1N3M pattern as viewed from cytosol, see text. The *thick arrows* in the open field indicate the progress of the rows of dimers, see Ref. [8]. In **b** the rows of dimers are oriented perpendicularly vs **a**, thus the RD monomers under the semitransparent Gtα units (*green*), which receive the Gtα(340–350) C-terminal tip (see below), are identically oriented in both the **a** and **b** models. This enables easy estimation of the difference in orientations of Gtα(340–350) in the RD* nests (e.g., by comparing the senses of the vectors αβ, see) as nearly opposite between both models, i.e., differing by ~150°. The coloring of RD monomers is rainbow-like according to sequence progression (N—*violet*, C—*red*) while the semitransparent Gtα, Gtβ and Gtγ are *green*, *yellow* and *blue*, respectively

slopes''. Clearly, this exhausts the four packing modes of a distorted ellipse, meeting 45°-compatible slopes. Slopes not ~45°-compatible (e.g., a ~90° slope, termed the ''H-IV'' arrangement [13–16]) were argued not to match the RD packing parameters typical of the array of rows of dimers revealed by AFM [9].

In this paper, we propose a supplementary arrangement of the 1HZX monomers into the paracrystalline array and a mode of Gt association to it, meeting all major experimentally proved constraints [17] and of possible general significance, see Fig. 1b. The Gt structure used in this work incorporates the Gtα(340–350) [18, 19] and Gtγ(60–71)farnezyl [20] C-termini in the conformations proven to stabilize MII. RD packing is achieved by the clockwise ~90° rotation of RD monomers in the 1N3M pattern viewed from cytosol, rearranging 1N3M into the combination of the ''45°/225° slopes'' mentioned above. Although the structure of activated RD (Meta II, MII) is unknown, its best-documented feature is a move of the cytosolic end of transmembrane helix 6, together with the associated N-terminal section of the cytosolic loop 3 (TM6/CL3, respectively), some 7–8 Å away from the heptahelical (7TM) bundle [17, 21, 22]. This feature is possibly common to all Class A GPCRs [23–25]. In the setup that we propose, TM6/CL3 have enough space to execute this move freely between the rows of dimers, see Figs. 1b and 2a, upon RD(GPCR) activation. Moreover, it is proven that ''dark''-to-MII activation of RD by light is entropy-driven at its final MI → MII step [26]. However, in the arrangement in Fig. 1a, any outward TM6/CL3 move, even if possible, must impose a very specific fold on CL3 to compromise its inevitable interference with an RD next in the row. This should considerably decrease entropy, contrary to experiment. Features of the proposed model are outlined and its experimental verifiability is discussed.

Methods

Gt interface likely compatible with MII

The almost complete Gtα(6–350) subunit was modeled through a fusion of the Gtαβγ·GDP X–ray structure [27] (PDB entry 1GOT) with the Gtα(340–350) C–terminal undecapeptide analog (PDB entry 1LVZ) in the conformation it assumes in the complex with RD* [19]. The fusion was accomplished via their overlapping region I340–K–E342, subsequent elimination of double residues from this region belonging to 1LVZ, and completed by the mutation S347C. Similarly, the almost complete Gtγ(9–71)farnezyl subunit was modeled through a fusion of the same Gtαβγ·GDP structure [27] (PDB entry 1GOT) with the Gtα C–terminal Gtγ(60–71)farnezyl dodecapeptide (PDB entry 1MF6) in a complex with RD* [20], via their overlapping region D60–K–N62, subsequent elimination of double residues from this

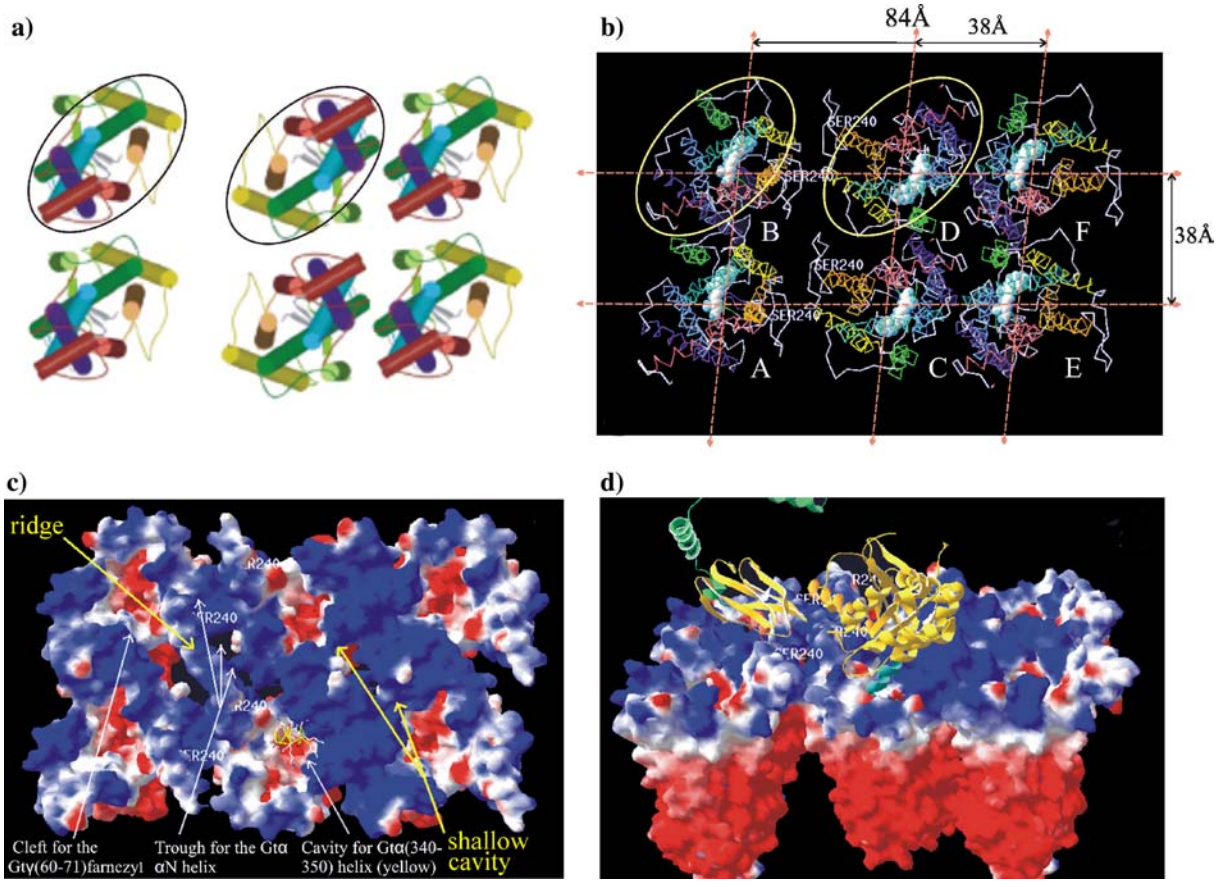

Fig. 2 **a** A scheme of the arrangement of RD monomers into the rows of dimers proposed in this work, as seen from the Gt perspective (exactly as in Fig. 1b). **b** Backbone trace of $(RD^*)_6$ modeled as described in "Methods" section, seen from the cytosol. In each monomer (A–F) the ultimate 20 C–terminal residues are truncated, which does not affect activation of the visual cascade [32] but greatly facilitates modeling. Notice that the apparent gaps seen in **a** have been plugged due to the execution of the TM6/CL3 move ~8 Å away of the 7TM bundle *in every* RD* monomer, see "Methods" section and Ref. [31]. The regular-structure elements (α and β) of RD monomers are colored rainbow-like according to sequence progression (N–*blue*, C—*red*) while irregular ones (loops) are *white*. The all-*trans* retinal is space-filled in *cyan*. **c** Potential surface of $(RD^*)_6$ viewed from the same perspective as in **b**. Notice the complementation of potentials with Gt, see Fig. 3. Major features of the interface for Gt are indicated in the drawing. **d** Overview of the $(RD)_6$–Gt complex described in the text. $(RD^*)_6$ is in the potential surface and Gt in ribbon projection. In Gt, the part of Gtβ drawn *red* in Fig. 3 top is omitted for clarity. The figure is rotated 60° around the horizontal axis, relative to Panel **c**. Notice the CL3–CL3 ridge "surrounded" by both *orange* Gtβ(280–340) and αN(6–26) [35]. Notice that, apart from the TM6/CL3 plug mentioned above, there is a crevice compatible with the separation of 46 Å (compare "Introduction" section) between the nearest units from adjacent rows of dimers

region belonging to 1GOT, and manual adjustments of the attached Gtγ(60–71)farnezyl C terminus into a position resembling those in Fig. 5 in Ref. [20] and Fig. 1 in Ref. [28], respectively. Gtβ of 1GOT was left intact. Finally, the so modified Gtαβγ· GDP was energy-minimized to remove van der Waals clashes using the Gromos96 force-field [29] as implemented in the SwissPDBView program [30], and as such ready for further use. All other modeling was also carried out using this program. This modified Gt as viewed from the receptor/membrane perspective is shown in Fig. 3 (top) and the molecular potential surface with major features at the RD^* –Gt interface is shown in Fig. 3 (bottom).

The "all-RD^*" hexamer

An RD_6 "unit cell", PDB code 1N3M, representative of the theoretical model of the native organization of RD, described using AFM by Liang et al. [8], was used as a start for the current model. This hexamer consists of two 3/2-dimers subsequent in the row, thus including two extra RD monomers from an adjacent row of dimers, superfluous from the viewpoint of definition of the unit cell but very useful from the viewpoint of explicit visualization of the interfaces within and between the dimers [8], see Figs. 1 and 2a. Subsequently, all RD monomers were rotated clockwise by 90°, as viewed from the cytosol, around their local bilayer-normal axes passing their local centers of gravity, to give the arrangement as in the hexamer in Figs. 1b and 2a (the "45°/225° slope"). In the next step, each 1HZX monomer in the hexamer was replaced with the putative RD* monomer (not shown), described in detail earlier [31]. Briefly, RD* consisted of the unbroken rhodopsin 1–327 sequence terminating six residues past the cytosolic helix 8, included the all-*trans*-retinal at K296 and TM6/CL3

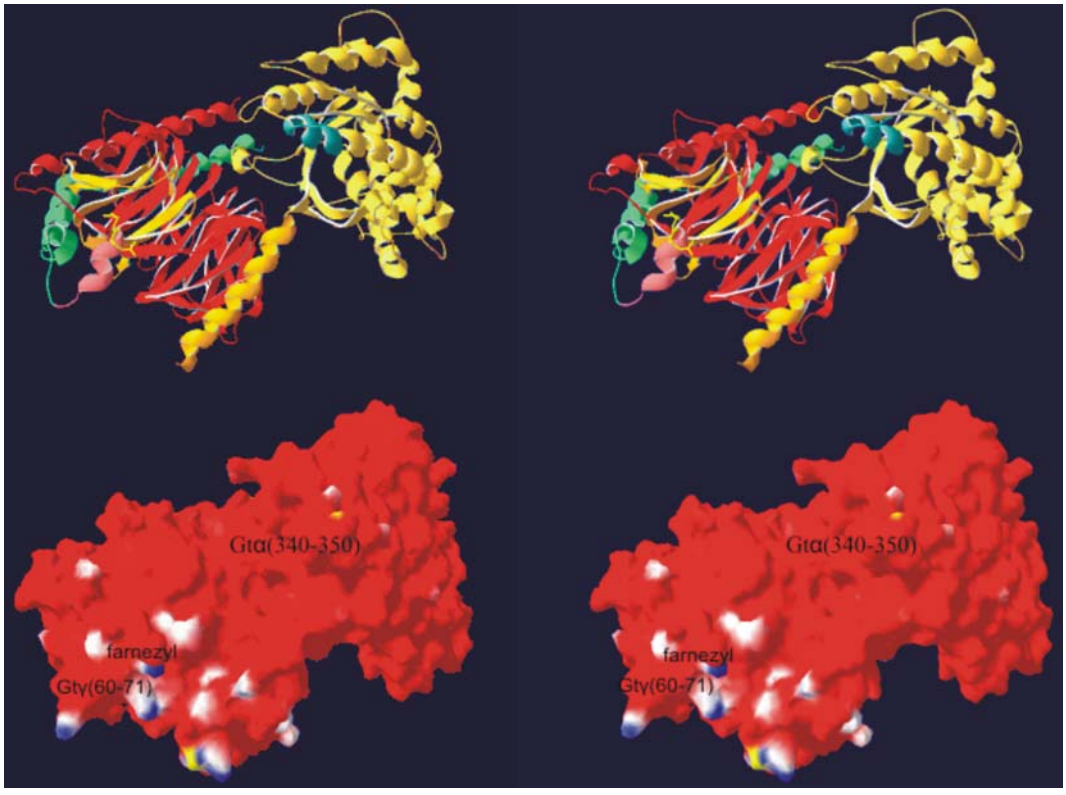

Fig. 3 Overviews in stereo of Gt modified as described in "Methods" section. Both views are from the common receptor/membrane perspective. *Top*: Ribbon projection. Gtα is *yellow*, except the αN(6–26) helix in *orange* and the Gtα(340–350) C-terminus in *cyan*. Gtβ is *red*, except its C-terminal Gtβ(280–340) sequence in *orange* like αN(6–26) to easier facilitate, see Fig. 2d, that both cradle RD* CL3 [35]. Gtγ is *green*, except Gtγ(60–71) C-terminus in *salmon* and the farnezyl covalently bound to Cys61 in *yellow*. *Bottom*: Potential surface projection. *Red* 1.8, *white* 0 and *blue* 1.8 (in kT/e units). Both Gtα and Gtγ C-terminal sites are marked, other are easily figured out with reference to the *Top*. Notice electrostatic potential complementation between Gt and RD*, compare Fig. 2c

moved ~8 Å away from the 7TM bundle. Since it has been proved that the truncation of 19 C-terminal amino-acid residues did not affect activation of the visual cascade [32], this truncation (of the poorly resolved RD(334–348) C-terminus in RD, PDB code 1N3M, [11]) greatly facilitated the modeling, leading to an MD-relaxed RD* monomer with a relatively flat surface for a smooth RD*–Gt interface and a cavity capable of receiving the C–terminal helical Gtα or Gtγ(farnezyl) extensions. For more details, see Ref. [31]. The current substitution was accomplished by imposing the best fit using the helices TM1–TM2, TM4–TM5 (i.e., those proven to be least altered and repositioned upon RD activation [21]) between each of the six RD-to-putative RD* pairs. Clearly, there is neither a good reason for all RDs to "get activated" at the same time nor a good reason for which fraction of them should get activated while the remainder should not. So the complete RD-to-RD* replacement in the unit serves at this stage the purpose to examine a possibility of simultaneous fitting of adjacent MII-like monomers within the tightly packed experimental network and subsequent open possibility for trying out diverse modes of Gt docking, see below. Finally, the "all-RD*" hexamer was energy-minimized in vacuo to remove steric clashes. An overview of the "all-RD*" hexamer as seen from the cytosol/Gt perspective is shown in Fig. 2b and its potential surface in the same view with its major features at the RD*–Gt interface is shown in Fig. 2c.

Docking

The docking of both structures was guided by experimental constraints from RD*–Gt crosslinking experiments, compiled in a few reviews [33, 34] including the most recent and complete one [17], at the same time having in mind surface and potential complementation of both Gt and the $(RD^*)_6$ model at their interface (see Figs. 2 and 3, respectively). The manual-visual docking was done using the SwissPDBView package [30]. The following chief experimental crosslinking constraints were required to be met simultaneously: (1) RD* CL3 should be located between Gtα αN and the Gtβ(280–340) C-terminus [35]; (2) Gtα(340–350) C–terminal peptide should be located in the RD* cavity [17, 19], resulting from the outward TM6/CL3 move away from the 7TM bundle as described above, including complementation between the hydrophobic residues [36]; (3) RD* CL3 S240 should be able to interact with both the Gtα α4–β6 loop [37] and the α N helix [38]. Since the latter two are separated by over 40 Å, clearly—vast RD

rearrangements aside—an interaction of Gt with more than one RD* monomer is implicated for meeting both the latter constraints at the same time. Remarkably in this context, a span of Gt is roughly double that of an RD monomer at their putative interface. Finally, the $(RD^*)_6$–Gt complex was energy-minimized to remove van der Waals clashes, and as such ready for further analysis and discussion in this work and as a start for more advanced MD simulations in future. Simultaneously, three other systems comprising ''activated receptor''–Gα C–terminal peptide were modeled, viz., vasopressin (VP) V1aR–Gq/11, V2R–Gs and oxytocin (OT) OTR–Gq/11, to examine and compare mutual complementation and consistency, regarding conserved residues at the GPCR–Gt interface within the Class A family.

Results

Overview of interfaces between the monomers and the surface implicated by the proposed packing

In the proposed ''all-RD*'' set-up, in which the TM6/CL3 sequences F228–C264 (from the beginning of CL3 to the hinge in the middle of TM6, respectively, see Ref. [31] for details), are moved ~8 Å away from the 7TM bundle, the gap between the rows of dimers, as viewed from the cytosolic side, becomes completely plugged while the cavity inside an RD* monomer opens, Fig. 2c. We would like to stress, as already indicated in the ''Materials and methods'' section, that there is no good reason for all RDs to be activated at the same time or to decide which fraction of them should be activated while the remainder should not. Thus, the complete RD?RD* replacement in the unit serves here nothing else than the purpose of examining a chance for simultaneous fitting adjacent MII-like monomers within the experimental network [8] and subsequent prospect for trying out diverse modes of Gt docking, see below. Any RD* sequence also comprises a rotation by ~40° (clockwise when viewed from the cytosol) of the TM6 cytosolic end [22] T242–C264. In Fig. 2b the axes cross the gravity centers of the monomers while the ellipses, marking two C2-related monomers from the adjacent rows of dimers, contour their cytosolic surface. Hence the former and the latter are apparently eccentric. Notice at the same time that in Panel 3B the TM6/CL3 sequences clearly stick outside both ellipses, contrary to the scheme in Panel 3A, entirely composed of the inactive monomers. While progressing extracellularly, these RD* monomers move gradually away of each other, see the crevice in Panel 3D, giving back space between the rows of dimmers, possibly to be filled by a lipid. On the other hand, the dimers (C–E and B–F units in Panel 3B) in this arrangement are tight and their interface consists of a long sequence involving TM1–TM2–TM3 (N-terminal part) with the connecting cytosolic and extracellular loops 1, CL1 and EL1, respectively. Also, the carbonyls of the palmitoyls acylating C233 and C323 just past Helix8 interact with E150–N151 in the CL2/TM4 tip, contributing reciprocally, i.e., doubly, to this interface. It is possible that this wealth of interacting residues on the dimer interface plus possible counterions could counterbalance an unfavorable aspect of the CL1–CL1 proximity, consisting of three double-positive charge contacts in the immediate reciprocal vicinity, viz., chains C–E and/or B–F (not shown): H65–R69, K67–K67 and R69–H65. Our sequence-homology analysis (not shown) indicates that an accumulation and mutual configuration of positively charged residues on CL1, as observed at this interface, is not a feature conserved over the Class A GPCRs. It is worth mentioning that a similar interface, although involving slightly rotated and translated monomers, referred to as the ''H-4'' interface (see ''Introduction'' section and Ref. [9]), was found for the squid RD reconstituted in its native membrane, using electron microscopy on the 2D crystals [13, 14]. This invertebrate RD, ~35% homologous with mammalian RDs and proven to have the same molecular architecture [13], appears less tightly packed in its 2D crystal lattice than the mouse RD [8, 9], as the size of an equivalent hexamer cell for the squid rhodopsin is 44 Å×98 Å [13] compared to 38 Å×82 Å for the latter, see above. The comparative tightness of the latter packing is another argument for a careful implementation of the high-resolution RD monomers into the semicrystalline rows of dimers, securing potential for lateral expansion of selected monomers at activation; see ''Discussion'' section.

Inspection of the $(RD^*)_6$ surface, see Fig. 2c, shows distinct cavities in the monomers, capable of receiving Gtα(340–350) and/or Gtγ(60–71)farnezyl. Between the rows of dimers these cavities extend into two parallel troughs separated from each other by a distinct diagonal NW–SE ridge, made two CL3s that protrude into the cytosol and interact as of a bridge and provided by their respective (B and C) diagonal RD*s, see Fig. 2c. This ridge fixes an edge for each trough on both sides, the other edge for each trough is provided by fragments of the CL2 and CL3 of the other pair of RD* (D and A for the upper-right and the lower-left troughs, respectively, see Fig. 2b, c).

Contrary to the space between the rows of dimers, where the diagonal ridge is a distinct feature, the space shared among a couple of dimers in the row is characterized by a relatively shallow trough also running NW–SE, from D to E RD* monomers, respectively in the pair of dimers, connecting their cavities, see Fig. 2c. Given Gtα(340–350) located in whatever RD* cavity [17–19, 36], one arrives at the conclusion that satisfying the requirements listed in the ''Docking'' section simultaneously needs Gt to be located over the RD* hexamer so that its long αN Gtα helix runs, sequence progressing, along the upper(right) NW–SE trough between the rows of dimers. At the same time, the Gtα(340–350) would fit e.g., the cavity of RD*(C) while Gtγ(60–71)farnezyl, especially the farnezyls—the site where the RD*(B)

cavity begins to extends into the lower(left) SE–NW trough, Fig. 2d. Clearly, an equivalent C2–symmetrically related $(RD^*)_6$–Gt docking in which Gtα(340–350) takes the RD*(B) cavity and the αN Gtα helix—the lower SE–NW trough, is equally possible. Any attempt to locate Gt over any pair of dimers, i.e., C–E(D–F) RD* monomers, is incompatible with the experimental requirements listed in the "Docking" section. Hence, from now on, locations of Gt over the two consecutive pairs of RD* monomers spanning the gap between the rows of dimers (A–C, B–D) are considered while the two far right partners in the dimers (E and F) are mostly ignored.

Selected details of the interfaces and docking

Details of the interface between the cytosolic loops 3 (CL3) involving three proximal RD* monomers A–C–B (compare Fig. 2) are shown in Fig. 4. This interface makes a background for Gt Gtα(340–350), shown as cyan ribbon entering RD*(C), Gt(60–71)farnezyl, shown as a salmon ribbon over the RD*(B) and Gtα αN(6–26) and selection of 60 C-terminal Gtβ(280–340) residues, both shown as an orange ribbon. Other parts of Gt are omitted in Fig. 4 for clarity. The non-conserved α N(6–26) helix, although essentially embedded on one side between the double-CL3 bridge, linking RD*(C) with RD*(B), and between fragments of CL2 and CL3 of RD*(D) on the other side, appears to be self-contained regarding most of its abundant ionic interactions. On the contrary, the non-conserved C–terminal Gtβ(280–340) sequence of the β-blade structure, shown fragmentarily in orange in Fig. 4 (compare also Figs. 2d and 3 for overviews), exposes only three (Gtβ:D312, Gtβ:D333, Gtβ:K337) ionic residues at the interface with the RD* A and B units on its left and right, respectively, and also to the CL3 tip of RD*(C). Putting more details aside (see "Discussion" section below), these CL3 proximities to both the α N(6–26) helix and the Gtβ(280–340) sheet are in agreement with Refs. [35, 37, 38].

The inter-RD* A–C (and/or B–D) interface consists of a pair of ionic K231–E232 cross-interactions embedded in the non-polar (V227, F228, A233) C2–quasi-symmetrical environment. On the other hand, the C–B interface consists of a pair of polar Q237–Q238 inter-chain cross-interactions, supported with intra-chain Q236–Q244 interactions. Q238 of chain A, apparently missing a partner, satisfies compensates by a polar-ionic interaction with Gtα R310 in the α4–β6 loop, again in agreement with experiment [37, 38]. The Gt(60–71)farnezyl helix in the upper-left corner manifests only one ionic interaction between its conserved K65 and RD*(C) E239 from CL3, while plugging itself a wide trench between CL3 and CL1, compatible with activated RD*(A).

Details of the RD*(C)–Gtα(340–350) environment are shown in Fig. 5. This is a side view, rotated −90° around the horizontal axis relative to the views in Figs. 2b, c and 4. Again, the receptor backbone is shown as the Cα-trace and the Gtα backbone is shown as a ribbon with the coloring retained from Figs. 2 and 4. Notice the following ion-pair interactions: between the conserved Gtα(340–350) residues and the receptor DRY motif (Gtα always first *in italic*): *K345*–E134 and *D346*–K134, as well as—unlabelled—in the upper-left corner and compatible with experiment [37, 38], between the α4–β6-loop *D311* and CL2 K141 (see their labels in another orientation in Fig. 4). Also notice the other conserved non-polar ones: *L344*–F313 and *L349* enclosed by M253 and M309. A possible involvement of the conserved TM7/H8 M309/F313, respectively, and TM6: in direct interactions with the Gtα C-terminus does not agree with the conclusions of Guo et al. [36] that RD activation exposes a key hydrophobic binding site, consisting of L226, T229 and V230 at the

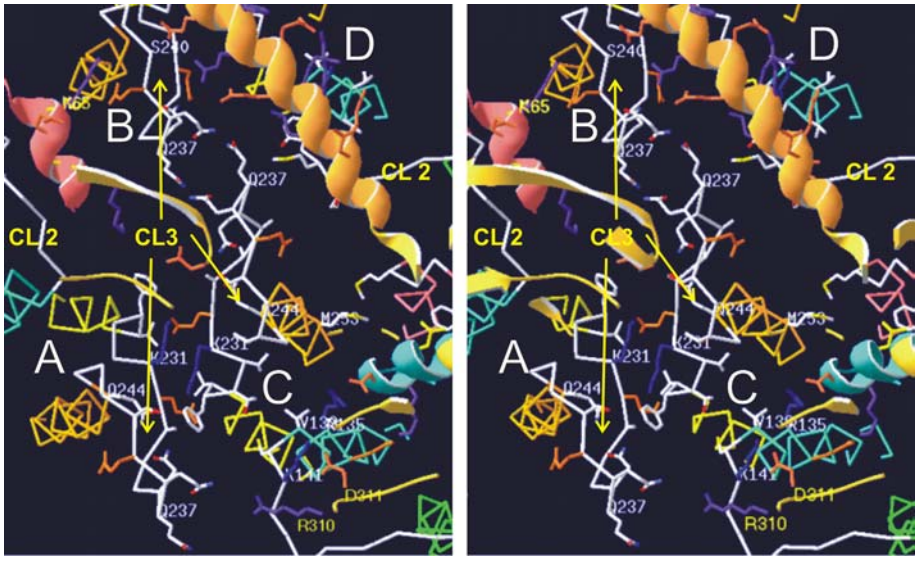

Fig. 4 Details of the putative interface between the cytosolic loops 3 of RD* A–B–C–D monomers in stereo (compare Fig. 2). RD* monomers are shown as the Cα trace with selected amino acids indicated. The coloring of RD* and Gt is the same as in Figs. 2b and 3 or 2d. This interface provides putative docks for Gt Gtα(340–350) in RD*(C), for Gt(60–71)farnezyl in RD*(B), for Gtα αN(6–26) and for the C-terminal Gtβ(280–340) residues. This is a *top view*, as in Figs. 1b and 2a–c. See text ("Results" section) for details

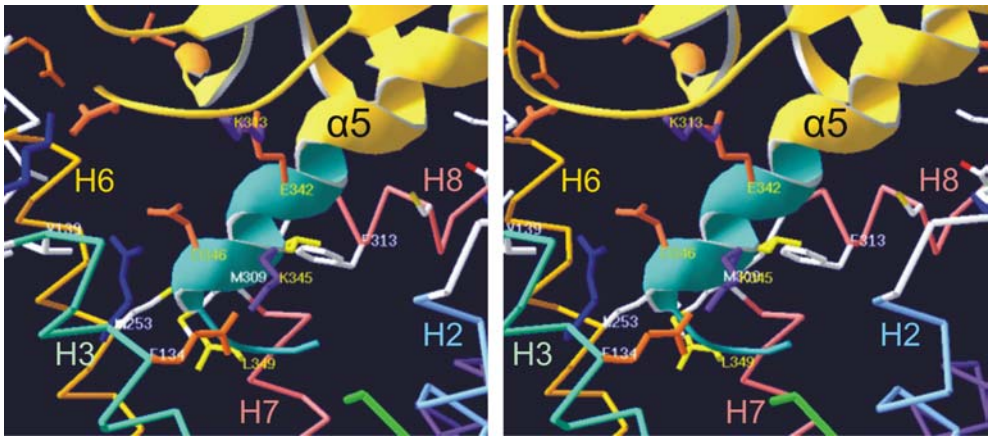

Fig. 5 Details of the RD*–Gtα(340–350) environment in stereo. This is a side view, rotated by −90° around the horizontal axis relative to the views in Figs. 1, 2a–c and 4. Proteins representation and coloring are as in Fig. 4. Selected side chains positioned for potential interactions with neighbors are indicated: acidic—in *red*, basic—in *blue*, RD* non-polar natural (CPK) and Gtα non-polar—*yellow*. Receptor labels are *white* while Gtα labels are *yellow*. See text ("Results" section) for details

N-terminus of CL3. In the proposed mutual RD*-Gt arrangement, Gtα(340–350) would arrive just from an opposite side relative to the site of these residues. Given the generality level of this hypothesis, agreements or disagreements regarding fine details of interactions may be fortuitous while attributing to them structural significance without solid experimental confirmations. Indeed, very recently an original newly crystallized bovine RD X-ray structure by Li and coworkers [39] (PDB entry 1GZM) and a forth refinement of bovine RD structure at atomic resolution by Okada et al. [40] (PDB entry 1U19; following the former entries 1F88, 1HZX and 1L9H, originating in Palczewski's lab [11, 41, 42], respectively) have been published. A novel and unique feature of both RD X-ray structures (1U19 and 1GZM), determined from different crystal space groups ($P4_1$ and $P3_1$, respectively), are complete for the first time, although marked by high thermal factors, densities for the intracellular domains, mutually differing mainly in the CL3, also divergent in this key loop from 1HZX [11], are prototypic for this hypothesis. Thus, this frame proposal would accordingly change in its details if either of the newest (1U19 and/or 1GZM) entries were taken as a start. See the "Discussion" section for more details. At any rate, the CL3 non-polar residues and those putatively indicated in Fig. 5 may provide screens embedding the sets of ion-pair interactions between RD* TM 3 E134 and R135 from the ERY sequence and conserved ionic counterparts from the Gtα C-terminus.

Discussion

The current model of RD* activation and interaction with Gt, resulting from attempts to assemble pieces of indirect data from biochemical experiments on binding sites involving interactions between RD* and Gt (and in other GPCR–G protein systems) coherently, is chiefly a hypothesis without a direct projection let alone confirmation in the explicit structure information. While there is a poor chance for resolving the structure of RD*(MII) (even more so other related activated GPCRs) in the foreseeable future due to the poor stability of the objects placed in extremely heterogenous natural environment, there is a chance for this (and other [12]) model(s) to evolve iteratively, even converge, to more precise ones, once indirect experimental data has filled gaps on mutual Class A GPCR–G protein interactions. Motivation for this is great, given over 50% drugs in use are mediated by GPCRs, making a very substantial part of the market [43].

However, it is as likely that no consensus general model for Class A GPCR activation is possible, i.e., exists. An argument for this could be the great diversity in sequences (both in lengths and composition) of the cytosolic loops 2 and 3 among the receptors, and the implicated mechanisms for GPCR–G protein signal transduction involving these loops. A good example for this is provided by documented facts that among the vasopressin receptors V1a and V2 (V1aR and V2R, involved in blood pressure and antiduresis, respectively) it is CL2 in V1aR that is responsible for the receptor binding to Gq/11 while CL3 in V2R central is to its binding to the Gs protein [44]. However, despite apparently quite different mechanisms involved as above in signal transduction at the GPCR–G protein interface employing non-conserved segments, it is possible that where conserved interactions are implicated, as possibly between the GPCR DRY sequence and Gα C-terminus (see e.g., [18]), there is good chance for iterative refinement and convergence to generalized aspects of GPCR–G protein interaction and signal transduction regarding at least Gtα(340–350) or the equivalent C-terminal sequence of any Gα segment into the respective activated Class A monomer. In this respect, it is worth mentioning that the mutual configuration between Gtα and its "own" RD* proposed in this work is very like that in an early model proposed by Bourne [33], utilizing then relatively scarce pieces of experimental constraints. Simultaneously, this hypothesis smoothly accommodates the well-documented role of the conserved (D/E)RY TM3 C-terminal sequence in activation and signal transduction among diverse representatives of Class A GPCRs.

On the other hand, neither this model nor the other one [12], in which Gtα is nested in its "own" RD* in a state rotated coaxial to the bilayer normal by about 150° (compare Fig. 1b with a), do not enable any explicit interactions between Gα C-terminal nonpolar residues and those indicated recently as possible RD hydrophobic binding site, i.e., L226, T229 and I230 at the N-terminal section of CL3. Both nearly opposite arrangements place the Gtα(340–350) peptide too far away from those residues for any direct contact. Again, the proven flexibility of the GPCR–G protein interface [17] may be a possible answer as to a chance of fulfilling this requirement. In this respect, the recent two new RD structure refinements [39, 40] (see above, PDB entries 1U19 and 1GZM at 2.2 and 2.65 Å resolution, respectively), although not undermining the basic concept of this or the other [12] hypothesis, may and will markedly affect details of the interfaces mentioned above. For this hypothesis, the 1HZX entry [11] was used, subsequently patched for the chain gap in CL3, and modeled to the putative RD* state [31]. However, 1HZX differs noticeably in CL3 from 1U19, which in turn quite dramatically differs in CL3 from 1GZM. Clearly, any attempted RD* modeled from either 1U19 or 1GZM would result in diverse molecular architectures in and around CL3. The RD cytosolic interface, CL3 in particular (and likely that of the whole Class A), is the most volatile part of a GPCR. This is confirmed in the largest thermal factors for these areas in the X-ray data of RD [11, 39–42]. This flexibility, which is a benefit for various GPCR–G protein specific cross-talk, is simultaneously a curse for structure studies at the interface between the two proteins.

Regarding the RD setups into the semicrystalline network [7–9], the current one is fairly similar within the intra-dimer interface to that found experimentally for squid RD using electron cryo-microscopy on the 2D crystals [13, 14]. The invertebrate RD, reconstituted into the native membrane, makes a regular network of pairs of dimers, noticeably looser than that of bovine RD found by AFM [8, 9]. Whereas the nearest-neighbor monomers of squid RD are mutually oriented antiparallel, those within the dimers stick parallel to each other in the C2 local symmetry, utilizing their TM4 for the interface of the "H-IV" type [9], i.e., in the "∼90° slope", see "Introduction" section. Indeed, an inspection of Fig. 3 in the paper of Davies et al. [13] with reference to Fig. 1b in this paper demonstrates that the monomers in the two dimers differ by less than 45° rotation and a mutual shift along the axes of rows of dimers, turning both TM4 as the main contributors to the interface within the squid RD dimer. An 8 Å resolution in the membrane plane neither leaves doubts for common 7TM structures of squid and bovine RD monomers nor as to the packing mode of the former [13]. This is in contrast to the AFM resolution, merely sufficient to reveal individual RD molecules and their packing parameters [8]. Clearly, looser packing into the rows of dimers of squid [13, 14] than mouse [8, 9] RD (reflected in the size of the equivalent hexamer cells equal to 44 Å×98 Å and 38 Å×82 Å, respectively) enables a ∼90° slope for the former and rules it out in the latter. Thus, it is tempting to notice that the "45°/225° slope" subject of this packing hypothesis for vertebrate RD could be a direct compromise requisite for squeezing the "H-IV" [9] (∼90° slope) type setup along both axes to meet packing constraints arriving at a change from the 44 Å×98 Å to 38 Å×82 Å dimensions of the RD-hexamer cell.

The present model meets most of the reported crosslink constraints [17, 19–22, 37, 38] and is compatible with simultaneous stabilization of Meta II by the C-termini of Gtα [18, 19] and Gtγ(farnezyl) [20]. The potential interactions between the latter two peptides and the respective RD* molecules implemented in the proposed model for RD oligomerization are all compatible with the CL3 movement and involve, where applicable, sets of residues conserved over Gtα/Gtγ and Class A. The sets of new interactions implicated by this hypothesis (e.g., at the RD* monomer interfaces, although experimentally verifiable [17]) are largely fortuitous. In view of the widespread functional (dimer-/oligomer)ization among this group of GPCRs, this hypothesis may be of general significance in the aspects involving conserved residues and a reasonable start for future iterative experimental-and-modeling refinements.

Acknowledgements Supported by KBN grant BW/8000-5-0260-5. Computational time in CI TASK, Gdańsk, and in ICM, Warsaw, is acknowledged.

References

1. Angers S, Salahpour A, Bouvier M (2002) Annu Rev Pharmacol Toxicol 42:409–435
2. Dean MK, Higgs C, Smith RE, Bywater RP, Snell CR, Scott PD, Upton GJG, Howe TJ, Reynolds CA (2001) J Med Chem 44:4595–4614
3. George SR, O'Dowd BF, Lee SP (2002) Nat Rev Drug Discov 1:808–820
4. Breitwieser GE (2004) Circ Res 94:17–27
5. Terrillon S, Bouvier M (2004) EMBO Rep 5:30–34
6. Bai M (2004) Cell Signal 16:175–186
7. Fotiadis D, Liang Y, Filipek S, Saperstein DA, Engel A, Palczewski K (2003) Nature 421:127–128
8. Liang Y, Fotiadis D, Filipek S, Saperstein DA, Palczewski K, Engel A (2003) J Biol Chem 278:21655–21662
9. Fotiadis D, Liang Y, Filipek S, Saperstein DA, Engel A, Palczewski K (2004) FEBS Lett 564:281–288
10. Berman HM, Westbrook J, Feng Z, Gilliland G, Bhat TN, Weissig H, Shindyalov IN, Bourne PE (2000) Nucleic Acids Res 28:235–242
11. Teller DC, Okada T, Behnke CA, Palczewski K, Stenkamp RE (2002) Biochemistry 40:7761–7772
12. Filipek S, Krzyśko KA, Fotiadis D, Liang Y, Saperstein DA, Engel A, Palczewski K (2004) Photochem Photobiol Sci 3:628–638
13. Davies A, Schertler GF, Gowen BE, Saibil HR (1996) J Struct Biol 117:36–44
14. Davies A, Gowen BE, Krebs AM, Schertler GF, Saibil HR (2001) J Mol Biol 314:455–463
15. Guo W, Shi L, Javitch JA (2003) J Biol Chem 278:4385–4388
16. Lee SP, O'Dowd BF, George SR (2003) Life Sci 74:173–180

17. Hubbel WL, Altenbach C, Hubbel CM, Khorana HG (2003) Adv Protein Chem 63:243–290
18. Kisselev OG, Kao J, Ponder JW, Fann YC, Gautam N, Marshall GR (1998) Proc Natl Acad Sci USA 95:4270–4275
19. Koenig BW, Kontaxis G, Mitchell DC, Louis JM, Litman BJ, Bax A (2002) J Mol Biol 322:441–461
20. Kisselev OG, Downs MA (2003) Structure 11:367–373
21. Altenbach C, Klein-Seetharaman J, Cai K, Khorana HG, Hubell WL (2001) Biochemistry 40:15493–15500
22. Farrens DL, Altenbach C, Yang K, Hubbel WL, Khorana HG (1996) Science 274:768–770
23. Shi L, Liapakis G, Xu R, Guarnieri F, Ballesteros JA, Javich JA (2002) J Biol Chem 277:40989–40996
24. Ghanouni P, Steeinhuis JJ, Farrens DL, Kobilka BK (2001) Proc Natl Acad Sci USA 98:5997–6002
25. Kostenis E, Conklin BR, Wess J (1997) Biochemistry 36:1487–1495
26. Okada T, Ernst OP, Palczewski K, Hofmann KP (2001) Trends Biochem Sci 26:318–324
27. Lambright DG, Sondek J, Bohm A, Skiba NP, Hamm HE, Sigler PB (1996) Nature 379:311–319
28. Herrmann R, Heck M, Henklein P, Henklein P, Kleuss C, Hofmann KP, Ernst OP (2004) J Biol Chem 279:24283–24390
29. van Gunsteren WF, Berendsen HJC (1996) Biomolecular simulation: Gromos96 manual and user guide. Vdf Hochschulverlag ETH Zürich (http://www.igc.ethz.ch/gromos/)
30. Guex N, Diemand A, Peitsch MC (1999) Trends Biochem Sci 24:364–367
31. Ślusarz R, Ciarkowski J (2004) Acta Biochim Pol 51:129–136
32. Komolov KE, Senin II, Filippov PP (2002) Rus J Bioorg Chem 28:16–22
33. Bourne HR (1997) Curr Opin Cell Biol 9:134–142
34. Meng EC, Bourne H (2001) Trends Pharmacol Sci 22:587–593
35. Taylor JM, Jacob-Mosier GG, Lawton RG, Remmers AE, Neubig RR (1994) J Biol Chem 269:27618–27624
36. Janz JM, Farrens DL (2004) J Biol Chem 279:29767–29773
37. Cai K, Itoh Y, Khorana HG (2001) Proc Natl Acad Sci USA 98:4877–4882
38. Itoh Y, Cai K, Khorana HG (2001) Proc Natl Acad Sci USA 98:4883–4887
39. Li J, Edwards PC, Burghammer M, Villa C, Schertler GFX (2004) J Mol Biol 343:1409–1438
40. Okada T, Sugihara M, Bondar A-N, Elstner M, Entel P, Buss V (2004) J Mol Biol 342:571–583
41. Palczewski K, Kumasaka T, Hori T, Behnke CA, Motoshima H, Fox BA, Le Trong I, Teller DC, Okada T, Stenkamp RE, Yamamoto M, Miyano M (2000) Science 289:739–745
42. Okada T, Fujiyoshi Y, Sillow M, Navarro J, Landau EM, Shichida Y (2002) Proc Natl Acad Sci USA 99:5982–5987
43. Klabunde T, Hessler G (2002) ChemBioChem 3:928–944
44. Liu J, Wess J (1996) J Biol Chem 271:8772–8778